Clinical Epigenetics

RESEARCH

Open Access

H3K18 lactylation-mediated *Ythdf2* activation restrains mouse female germline stem cell proliferation via promoting *Ets1* mRNA degradation

Yunqiang Wu[1†], Bo Xu[4†], Yonglin Peng[1], Sang Lin[1], Wenfei Du[1], Ruiqi Liu[1], Shu Zhang[2,3], Ji Wu[4], Kang Zou[2,3*] and Xiaodong Zhao[1*]

Abstract

Background Germline stem cells are critical for sustaining fertility by balancing self-renewal and differentiation, and are regulated by genetic and epigenetic programs. Although extensively investigated, the rare female germline stem cells (FGSCs) in mammalian ovaries hinder their application in regenerative medicine. The N^6-methyladenosine (m^6A) reader YTHDF2 is required for female germ cell competence. However, the mechanistic underpinnings of how YTHDF2 regulates FGSC proliferation remain elusive.

Results Here, we show that knockout of *Ythdf2* enhances FGSC proliferation in vitro. YTHDF2 binds m^6A-modified *Ets1* mRNA and facilitates its degradation in an m^6A-dependent manner. ETS1 functions as a key downstream effector of YTHDF2, as suppression of ETS1 expression partially reverses the *Ythdf2*-KO-induced phenotype. Additionally, we demonstrate that YTHDF2/ETS1 axis participates in regulating FGSC proliferation by modulation of proliferation-related gene expression. Moreover, histone lactylation modification H3K18la activates the expression of YTHDF2 in FGSCs.

Conclusions Overall, our study reveals that YTHDF2 intrinsically restrains mouse FGSC proliferation and provides a potential strategy to increase FGSC abundance for its potential clinical application.

Keywords Female germline stem cell, N^6-methyladenosine, YTHDF2, ETS1, Histone lactylation

†Yunqiang Wu and Bo Xu have contributed equally to this work.

*Correspondence:
Kang Zou
kangzou@njau.edu.cn
Xiaodong Zhao
xiaodongzhao@sjtu.edu.cn
[1] Key Laboratory of Systems Biomedicine (Ministry of Education), Shanghai Center for Systems Biomedicine, Shanghai Jiao Tong University, Shanghai, China
[2] College of Animal Science and Technology, Nanjing Agricultural University, Nanjing, China
[3] Stem Cell Research and Translation Center, Nanjing Agricultural University, Nanjing, China
[4] Key Laboratory for the Genetics of Developmental and Neuropsychiatric Disorders (Ministry of Education), Bio-X Institutes, School of Medicine, Shanghai Jiao Tong University, Shanghai 200240, China

Introduction

Infertility has emerged as a pressing global issue, affecting an estimated 8–12% of reproductive-aged couples worldwide [1]. The female factors contribute to approximately 37% of infertility cases [2]. A shortage and poor quality of oocytes are key factors leading to female infertility. Female germline stem cells (FGSCs), residing within the cortex of postnatal ovaries, serve as precursors to oocytes and possess the capacity to proliferate and differentiate into functional oocytes, ultimately yielding fertile offspring [3, 4]. This unique attribute underscores the therapeutic promise of FGSCs in replenishing the exhaustion of follicle pool, thereby potentially restoring ovarian function, enhancing fertility, and improving pregnancy rates in clinical settings. However, the limited number of FGSCs in the mammalian ovary [5] presents a significant hurdle to their widespread clinical application. FGSC proliferation is orchestrated by intricate genetic and epigenetic programs, yet the precise mechanisms underlying their coordinated regulation remain elusive.

N^6-methyladenosine (m^6A), the most prevalent epigenetic modification in mammalian mRNA, is associated with RNA splicing, stability, translation, and nuclear export [6–9]. The m^6A modification is catalyzed by m^6A methyltransferases (writers), removed by m^6A demethylases (erasers), and recognized by m^6A-binding proteins (readers) [10–12]. The accumulating studies have reported that these m^6A regulators exert important effects on germ cell development. For instance, METTL3, a key m^6A methyltransferase, is required for oocyte meiotic maturation, and its deficiency leads to defective follicle development and abnormal ovulation [13]. Oocyte-specific deletion of *Kiaa1429,* another component of the m^6A methyltransferases, impairs follicular development and results in female mouse infertility [14]. Conditional knockout of *Ythdc1* is associated with oocyte maturation arrest and female mouse infertility [15]. Our recent studies have revealed that YTHDF1 regulates FGSC self-renewal [16]. Notably, *Ythdf2* is also highly expressed in FGSCs [16], whereas the function is not clear. YTHDF2 is known for the effect on the stability of m^6A-modified RNAs by localizing them to mRNA decay sites [7], and a study demonstrates that it is required for oocyte competence since its deficiency leads to female mouse infertility [17].

Despite these compelling insights, a comprehensive understanding of the molecular mechanisms by which m^6A regulators govern FGSC proliferation remains limited. In this study, we investigate the role and molecular underpinnings of YTHDF2 in FGSCs by perturbing its expression and analyzing the impact on cell fate and associated epigenetic events. Our results indicated that YTHDF2 serves as a negative regulator of FGSC proliferation, and histone lactylation promotes the transcription of *Ythdf2*. Mechanistically, YTHDF2 binds m^6A-modified mRNA encoded by transcription factor *Ets1* and triggers the degradation of *Ets1* mRNA. Consequently, ETS1-induced proliferation-related genes are down-regulated, resulting in proliferation suppression. This study provides novel insights into how m^6A regulators intrinsically restrain FGSC proliferation and potential therapeutic approaches for infertility.

Materials and methods

Cell culture

The FGSC line was established from mice as described in our previous report [3]. The FGSC line at passage number 25–35 was cultured according to our previous method [3]. Briefly, FGSCs were cultured on STO feeder cells using minimum essential medium-α (MEM-α, Life Technologies, USA), supplemented with 10% fetal bovine serum (FBS, Gibco, USA), 1 mM sodium pyruvate (Sigma, USA), 1 mM nonessential amino acid (NEAA, Gibco, USA), 2 mM L-glutamine (Invitrogen, USA), 0.1 mM β-mercaptoethanol (Sigma, USA), 10 ng/mL mouse epidermal growth factor (EGF, Pepro Tech, USA), 10 ng/mL mouse leukemia inhibitory factor (LIF, Pepro Tech, USA), 40 ng/mL mouse glial cell line-derived neurotrophic factor (GDNF, Pepro Tech, USA), 10 ng/mL human basic fibroblast growth factor (bFGF, Pepro Tech, USA), and 1% penicillin–streptomycin (Sangon Biotech, China). STO cells were cultured in Dulbecco's modified Eagle's medium (DMEM, Corning, USA) supplemented with 10% FBS, 1 mM NEAA, and 1% penicillin–streptomycin (Sangon Biotech, China). All cells were maintained at 37 °C in a 5% CO_2 incubator.

Generation of stable cell lines

The lentiviral vector pLentiCRISPR v2-sg*Ythdf2* was constructed for *Ythdf2* knockout. Similarly, the lentiviral vector pLKO.1-sh*Ets1* was constructed for ETS1 knockdown (KD). The related sequences of sgRNA and short hairpin RNA (shRNA) are listed in Supplementary file 1: Table S1. Wild-type (YTHDF2-WT) or m^6A-binding site-mutated (YTHDF2-Mut) of YTHDF2 were cloned into pSIN vector for YTHDF2 expression. HEK293T cells were used for lentiviral production and supernatant was collected at 48 and 72 h following transfection. The viruses were filtered using 0.45 μm filters, and appropriate quantities of viruses were employed to infect FGSCs. Subsequently, FGSCs were subjected to selection with puromycin (1 μg/mL) or hygromycin B (100 μg/mL) for 7–14 days. Finally, single cell-derived colonies were expanded and subjected to western blotting validation.

Immunofluorescence

Cells were fixed with 4% paraformaldehyde (PFA, Sangon Biotech, China) for 10 min, washed twice with phosphate-buffered saline (PBS), and blocked with 5% BSA for 30 min. Then cells were incubated with anti-MVH antibody (1:100, Abcam, Cat# ab13840) followed by a second antibody. Finally, cells were counterstained with DAPI solution (Sigma, USA) and viewed with a Nikon A1Si confocal microscope.

Western blotting analysis

Cells were lysed with ice-cold RIPA buffer (Thermo Fisher, USA) containing protease inhibitor cocktail (Roche, Switzerland). The protein concentrations were determined using BCA Assay protein Kit (Thermo Fisher, USA). Equal amounts of lysates were separated by 10% SDS-PAGE and then transferred onto PVDF membranes (Millipore, USA). The membranes were blocked with 5% nonfat milk for 1 h at room temperature followed by overnight incubation with primary antibody at 4 °C. After incubation with HRP-conjugated secondary antibodies for 1 h at room temperature, immunoblots were visualized using ECL Western Blotting Detection Kit (Thermo Fisher, USA). Antibodies used were as follows: anti-YTHDF2 (1:4000, Proteintech, Cat# 24744-1-AP), anti-ETS1 (1:3000, Proteintech, Cat# 12118-1-AP), anti-GAPDH (1:5000, Sangon Biotech, Cat# D110016), pan anti-Kla (1:1000, PTM BIO, Cat# PTM-1401RM), anti-H3K18la (1:2000, PTM BIO, Cat# PTM-1406RM), and anti-actin (1:20000, Proteintech, Cat# 66009-1-Ig).

Reverse transcription polymerase chain reaction (RT-PCR) and real-time quantitative polymerase chain reaction (RT-qPCR)

Total RNA was extracted from FGSCs using Trizol (Invitrogen, USA) following the manufacturer's instructions. Reverse transcription was conducted using PrimeScript^{TM}RT reagent Kit with gDNA Eraser (TAKARA, Japan) according to the manufacturer's protocol. *Gapdh* was employed as an internal control. Primer sequences are listed in Supplementary file 1: Table S2, S3.

Cell proliferation assay

Cells were seeded at a density of 1000 cells per well in 96-well plates. The proliferation rates were assessed at 24, 48, and 72 h using Cell Counting Kit-8 (CCK-8) reagent (Sangon Biotech, China) following the manufacturer's protocol.

EdU assay

Cells were incubated with 20 μM EdU agent for 2 h and subjected to staining using Click-iT EdU-488 Cell Proliferation Detection Kit (Servicebio, China) according to the manufacturer's instructions. Cell nuclei were stained with DAPI solution.

Cell cycle analysis

Cells were washed with ice-cold PBS and then fixed with 70% pre-cooled ethanol overnight at −20 °C. Afterward, cells were washed again with ice-cold PBS and resuspended in PBS containing 10 μg/mL RNase A (Thermo Fisher, USA) and 50 μg/mL propidium iodide (Thermo Fisher, USA). Subsequently, the cell suspension was incubated in the dark at 37 °C for 30 min. Cell cycle analysis was performed using BD LSRFortessa flow cytometer (BD Biosciences, USA).

TUNEL staining

Cells were placed on microscope slides (Liusheng, China) and subjected to staining using CF488 TUNEL Cell Apoptosis Detection Kit (Servicebio, China) according to the manufacturer's instructions. Cell nuclei were stained with DAPI solution.

RNA sequencing (RNA-seq) and analysis

RNA-seq library construction were conducted as we described previously [18]. Total RNA was extracted using Trizol (Invitrogen, USA) and then purified using NEBNext Poly(A) mRNA Magnetic Isolation Beads (NEB, USA) following the manufacturer's guidelines. Subsequently, the NEB Next Ultra Directional RNA Library Prep Kit (NEB, USA) was employed for library preparation. The mRNA library was then sequenced using an Illumina HiSeq 2000 platform (Illumina, USA).

The raw paired-end sequencing reads were processed using Trim-Galore (Version 0.6.7, available at https://github.com/FelixKrueger/TrimGalore). Subsequently, the qualified reads were mapped to the mouse genome (mm10) using HISAT2 (version 2.2.1, https://github.com/DaehwanKimLab/hisat2) with default parameters. Gene expression levels were calculated by featureCounts (version 2.0.1) and transformed into Fragments Per Kilobase of exon per Million fragments mapped (FPKM). The differentially expressed mRNAs were calculated by R package DESeq2, and those with $\log_2$ (fold change) > 1 or $\log_2$ (fold change) < -1, and p value < 0.05 were significantly differentially expressed genes.

Methylated RNA immunoprecipitation sequencing (MeRIP-seq) and MeRIP-qPCR

The experiments were conducted as previously described with some adjustments [6]. In brief, total RNA was extracted from FGSCs using Trizol and fragmented into 200-nt fragments with RNA Fragmentation Reagents. Subsequently, fragmented RNA was subjected to

immunoprecipitated using Protein A/G Magnetic beads (Millipore, USA) coupled with 3 μg anti-m^{6}A antibody (Synaptic Systems, Cat# 202 003), and then, m^{6}A RNA was purified using a NEBNext® rRNA Depletion Kit (NEB, USA). The purified m^{6}A RNA was used for either MeRIP-qPCR or library construction employing NEB Next Ultra Directional RNA Library Prep Kit (NEB, USA). Libraries were subjected to Illumina Hiseq 2000 for sequencing. Primer sequences utilized for MeRIP-qPCR are listed in Supplementary file 1: Table S3.

Bioinformatics analysis of MeRIP-seq data

Trim-Galore was employed for filtering out the reads with low quality. Subsequently, the qualified reads were mapped to the mouse genome (mm10) using HISAT2 with default parameters. DeepTools (version 3.5.2, https://github.com/deeptools/deepTools) was used to generate bigwig format files of mapped reads from both IP and input libraries. MACS2 (version 2.2.7.1) was employed for peak calling with default parameters. Additionally, the identified peaks were annotated with annotatePeaks.pl in HOMER toolkits (version 4.11). Peak regions were submitted to STREME in MEME suite (https://meme-suite.org/meme/tools/streme) to perform discriminative motif discovery.

RNA immunoprecipitation-qPCR (RIP-qPCR)

RIP-qPCR was performed as previously described with some modifications [19]. Briefly, FGSCs were lysed in IP lysis buffer and then incubated with anti-YTHDF2 antibody (Proteintech, China) for immunoprecipitation. Subsequently, the RNA–protein complex was extracted by Trizol, ethanol-precipitated with glycogen (Invitrogen, USA). cDNA was prepared using PrimeScript^{TM}RT reagent Kit with gDNA Eraser (TAKARA, Japan) following the manufacturer's protocol. Primer sequences used for RIP-qPCR are listed in Supplementary file 1: Table S3.

RNA stability assay

Cells were treated with 10 μg/mL of actinomycin D (Act D, Sigma, USA) and collected at 0, 2, 4, and 6 h. Subsequently, total RNA was extracted and subjected to RT-qPCR analysis after reverse transcription.

Chromatin immunoprecipitation coupled with qPCR (ChIP-qPCR)

ChIP experiments were performed as previously described [20]. Briefly, cells were cross-linked using 1% formaldehyde in PBS for 10 min and quenched with 125 mM glycine for 5 min. Immunoprecipitation of fragmented chromatin fragments was carried out using Protein A/G Magnetic beads (Millipore, USA) coupled with anti-ETS1 (Proteintech, Cat# 12,118–1-AP) and anti-H3K18la (PTM BIO, Cat# PTM-1406RM) antibody. The results were normalized to the input DNA and analyzed with the ΔΔCT method. Primer sequences used for ChIP-qPCR are listed in Supplementary file 1: Table S4.

Statistical analysis

All data were statistically analyzed and presented as mean ± SD. Statistical significance was calculated using Student's t-test. All experiments were conducted at least three times. The p value < 0.05 was regarded as statistically significant, and asterisks denote statistical significance (*$p < 0.05$, ** $p < 0.01$, *** $p < 0.001$, and **** $p < 0.0001$, n.s. $p >= 0.05$).

Results

YTHDF2 restrains FGSC proliferation in vitro

We first characterized the cultured FGSCs by examining morphological features and the molecular markers associated with germline development. The cultured cells form clusters with a bead-like shape (Fig. 1a) and are positive for the germline-specific marker MVH (Fig. 1b). Furthermore, we found that the cultured FGSCs express other germline markers, including *Fragilis*, *Stella*, *Oct4*, and *Dazl* (Fig. 1c). These observations suggest that the cultured FGSCs maintain the biological characteristics of primary isolated FGSCs, as we previously described [3].

To explore the role of YTHDF2 in FGSCs, we utilized the CRISPR/Cas9 genomic editing technique to establish a *Ythdf2*-KO FGSC line and observed a complete absence of YTHDF2 expression in the *Ythdf2*-KO cells (Fig. 1d). Subsequently, we examined cell viability and found that cell viability is significantly increased in *Ythdf2*-KO cells (Fig. 1e). Consistently, we also observed a higher proportion of EdU-positive FGSCs in *Ythdf2*-KO cells compared to wild-type (WT) cells (Fig. 1f, Supplementary file 1: Fig. S1A). These findings indicate that knockout of *Ythdf2* enhances FGSC proliferation. Additionally, we noted significant variations in cycle distribution in *Ythdf2*-KO cells, characterized by an increase in the S and G2/M phases, but a decrease in the G0/G1 phase (Fig. 1g, Supplementary file 1: Fig. S1B). Furthermore, depletion of *Ythdf2* significantly inhibits cell apoptosis (Fig. 1h, Supplementary file 1: Fig. S1C). Since genome editing possibly involves off-targets, we then applied DC-Y13-27 [21], a YTHDF2 inhibitor, to evaluate its effect on cell proliferation. After 72 h of treatment with DC-Y13-27, we also observed the promotion of cell proliferation (Fig. 1i). Taken together, these results demonstrate that YTHDF2 acts as a repressor of FGSC proliferation.

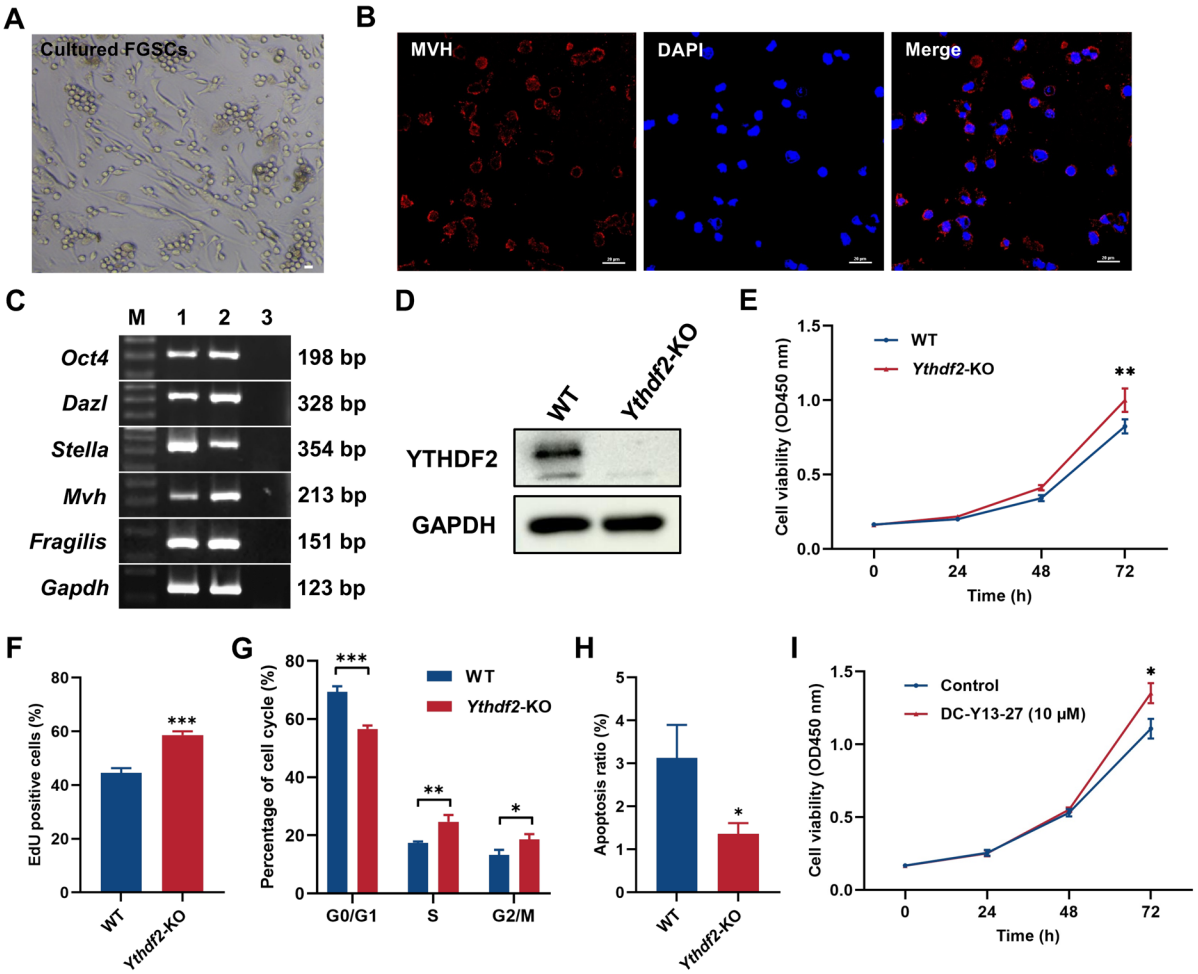

Fig. 1 YTHDF2 restrains FGSC proliferation in vitro. **a** Representative morphology of cultured FGSCs. Scale bar, 20 μm. **b** Immunostaining of MVH (red) in FGSCs. Nuclei were counterstained with DAPI (blue). Scale bar, 20 μm. **c** RT-PCR analysis for the cultured FGSCs. M, 100 bp DNA marker; lane 1, adult ovary; lane 2, FGSCs; lane 3, mock-transcribed FGSC RNA samples. **d** Western blotting analysis of YTHDF2 expression in WT and *Ythdf2*-KO cells. **e** Cell viability of WT and *Ythdf2*-KO cells was detected using CCK-8 assay. **f** EdU staining of WT and *Ythdf2*-KO cells. **g** Cell cycle analysis of WT and *Ythdf2*-KO cells using flow cytometry. **h** TUNEL staining of WT and *Ythdf2*-KO cells. **i** Cell viability of WT cells treated with or without DC-Y13-27 was detected using CCK-8 assay. *$p < 0.05$, ** $p < 0.01$, *** $p < 0.001$. Data are shown as mean ± SD

YTHDF2 functions to suppress m^{6}A-modified transcripts involved in cell proliferation

To understand the underlying molecular mechanism of YTHDF2, we conducted RNA-seq analysis in both WT and *Ythdf2*-KO FGSCs. Compared with the WT, a total of 1,283 genes were found to be differentially expressed in *Ythdf2*-KO cells, including 789 up-regulated genes and 494 down-regulated genes (Fig. 2a). Considering YTHDF2 primarily facilitates the decay of its target mRNAs, we thus focused on the up-regulated genes upon *Ythdf2* depletion. Gene ontology (GO) enrichment analysis indicates that the GO items of cell cycle, DNA replication, and cell division are enriched among the up-regulated genes (Fig. 2b). Additionally, gene set

(See figure on next page.)

Fig. 2 YTHDF2 negatively regulates cell proliferation. **a** Volcano plot representing the $\log_2$ fold change of differentially expressed genes upon *Ythdf2* depletion. **b** GO enrichment analysis of genes up-regulated in *Ythdf2*-KO cells. **c** GSEA plots showing the pathways of genes up-regulated in *Ythdf2*-KO cells. **d** m^{6}A motif was detected by the HOMER motif analysis with MeRIP-seq data in WT cells. **e** Pie chart presenting the distribution of m^{6}A peaks in the indicated regions in WT cells. **f** Metagene profiles of m^{6}A enrichment across mRNA transcriptome in WT cells. **g** Venn diagram showing the number of shared genes between MeRIP-seq and RNA-seq. **h** GO enrichment analysis of 146 overlapped genes described in (**g**)

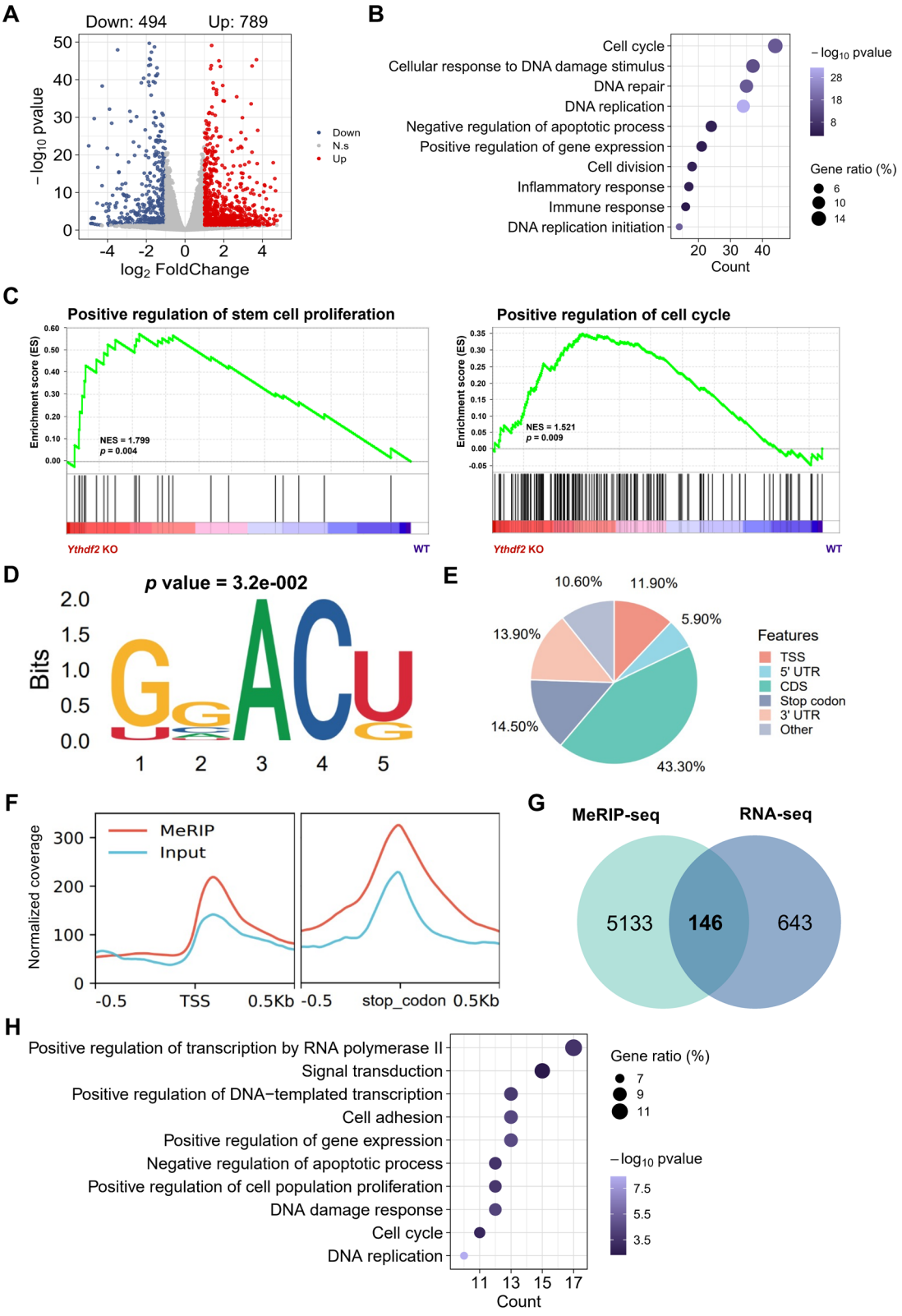

Fig. 2 (See legend on previous page.)

enrichment analysis (GSEA) shows significant up-regulation of positive regulation of stem cell proliferation and positive regulation of cell cycle (Fig. 2c). These findings implicate that YTHDF2 negatively regulates FGSC proliferation. YTHDF2 is widely recognized as an m^{6}A reader that binds to and destabilizes transcripts with m^{6}A modifications [22]. We next sought to identify the potential YTHDF2 target transcripts through MeRIP-seq analysis. We identified 7,871 m^{6}A modification sites associated with 5,279 genes. Using MEME algorithm, we observed the m^{6}A consensus motif (GGAC) enrichment in the m^{6}A peak (Fig. 2d). These m^{6}A modifications are predominantly located in protein-coding transcripts and enriched near the stop codons (Fig. 2e, f). To examine the effect of YTHDF2 on the expression of m^{6}A-modified transcript, the MeRIP-seq data were intersected with RNA-seq data, yielding m^{6}A-modified transcripts encoded by 146 genes which are up-regulated upon *Ythdf2* depletion (Fig. 2g). Consistently, GO enrichment analysis also shows GO items of positive regulation of cell population proliferation, cell cycle, and DNA replication are enriched in these 146 genes (Fig. 2h). These findings further indicate the inhibitory role of YTHDF2 in FGSC proliferation.

YTHDF2 destabilizes *Ets1* mRNA in an m^{6}A-dependent manner

To identify the downstream targets involved in YTHDF2 function among 146 up-regulated genes, the published YTHDF2 cross-linking immunoprecipitation and high-throughput sequencing (CLIP-seq) dataset from mouse T cells [23] was intersected with our MeRIP-seq data, yielding 20 up-regulated genes that have at least one m^{6}A site with potential YTHDF2-binding sites (Fig. 3a, Supplementary file 1: Table S5). Among these genes, *Ets1*, *Mcm3*, and *Ccna2* have been reported to promote cell proliferation [24–26], and their transcripts are m^{6}A-modified (Fig. 3b). Among these m^{6}A-modified transcripts, the m^{6}A modification level of *Ets1* exhibits a significant increase upon *Ythdf2* knockout (Fig. 3c). Furthermore, only *Ets1* mRNA is significantly enriched in YTHDF2 immunoprecipitation, indicating the binding of *Ets1* mRNA by YTHDF2 (Fig. 3d). These findings suggest *Ets1* as a target of YTHDF2 in FGSCs. To understand how YTHDF2 affects *Ets1*, we examined the transcription and translation status of *Ets1* upon *Ythdf2* knockout. As expected, depletion of *Ythdf2* increases both mRNA and protein levels of *Ets1* (Fig. 3e, f). Given that YTHDF2 targets tend to have short half-lives, we conducted RNA stability assay in WT and *Ythdf2*-KO FGSCs and found a substantial decrease in the degradation rate of *Ets1* mRNA in *Ythdf2*-KO cells compared to WT cells (Fig. 3g).

To ascertain that YTHDF2 regulates *Ets1* expression in an m^{6}A-dependent manner, we introduced one-point mutation W432A in the YTH domain of YTHDF2 (YTHDF2-Mut) [27], and then transfected FGSCs with either YTHDF2-WT or YTHDF2-Mut constructs. Cells transfected with YTHDF2-WT show a significant increase in *Ets1* mRNA enrichment, while marginal increase in YTHDF2-Mut cells (Fig. 3h). Furthermore, we observed that the mRNA level of *Ets1* is reduced in YTHDF2-WT, rather than YTHDF2-Mut cells (Fig. 3i). Collectively, these findings demonstrate that YTHDF2 destabilizes *Ets1* mRNA in an m^{6}A-dependent manner.

ETS1 serves as a key downstream effector of YTHDF2 in FGSCs

To understand the role of ETS1 in FGSCs, we utilized *Ets1* shRNA to knock down ETS1 expression in WT or *Ythdf2*-KO FGSCs (Fig. 4a, b). ETS1 KD significantly impedes cell proliferation, induces cell cycle arrest at the G0/G1 phase, and triggers cell apoptosis in WT FGSCs (Fig. 4c–f, Supplementary file 1: Fig. S2A—C). Meanwhile, we found that suppression of ETS1 expression partially reverses the *Ythdf2*-KO-induced phenotype, including proliferation inhibition, cell cycle arrest, and cell apoptosis (Fig. 4c–f, Supplementary file 1: Fig. S2A—C). These findings indicate that ETS1 serves as a key downstream effector of YTHDF2 in regulating FGSC proliferation.

YTHDF2/ETS1 axis participates in the regulation of FGSC proliferation

Transcription factor ETS1 exerts its effect by binding its genomic targets to modulate expression of target genes. To further understand the role of YTHDF2/ETS1 axis in FGSCs, we performed motif scanning analysis of ETS1 on YTHDF2-induced up-regulated genes with FIMO [28] and found that more than 70% of genes contain ETS1-binding sites (Fig. 5a). GO enrichment analysis shows that the GO items of cell cycle and positive regulation of cell proliferation are enriched among these ETS1 potential target genes (Fig. 5b, c). Based on these findings, we reasoned that *Ythdf2* deficiency unleashes ETS1 expression, resulting in up-regulation of ETS1 target genes and promoting FGSC proliferation. To support our speculation, we examined the status of expression and ETS1 binding of proliferation-associated genes using RT-qPCR and ChIP-qPCR. We observed a significant up-regulation of all the selected genes upon *Ythdf2* knockout in FGSCs with a significant increase in ETS1 binding (Fig. 5d, e). Collectively, these results demonstrate the role of YTHDF2/ETS1 axis in the negative regulation of FGSC proliferation.

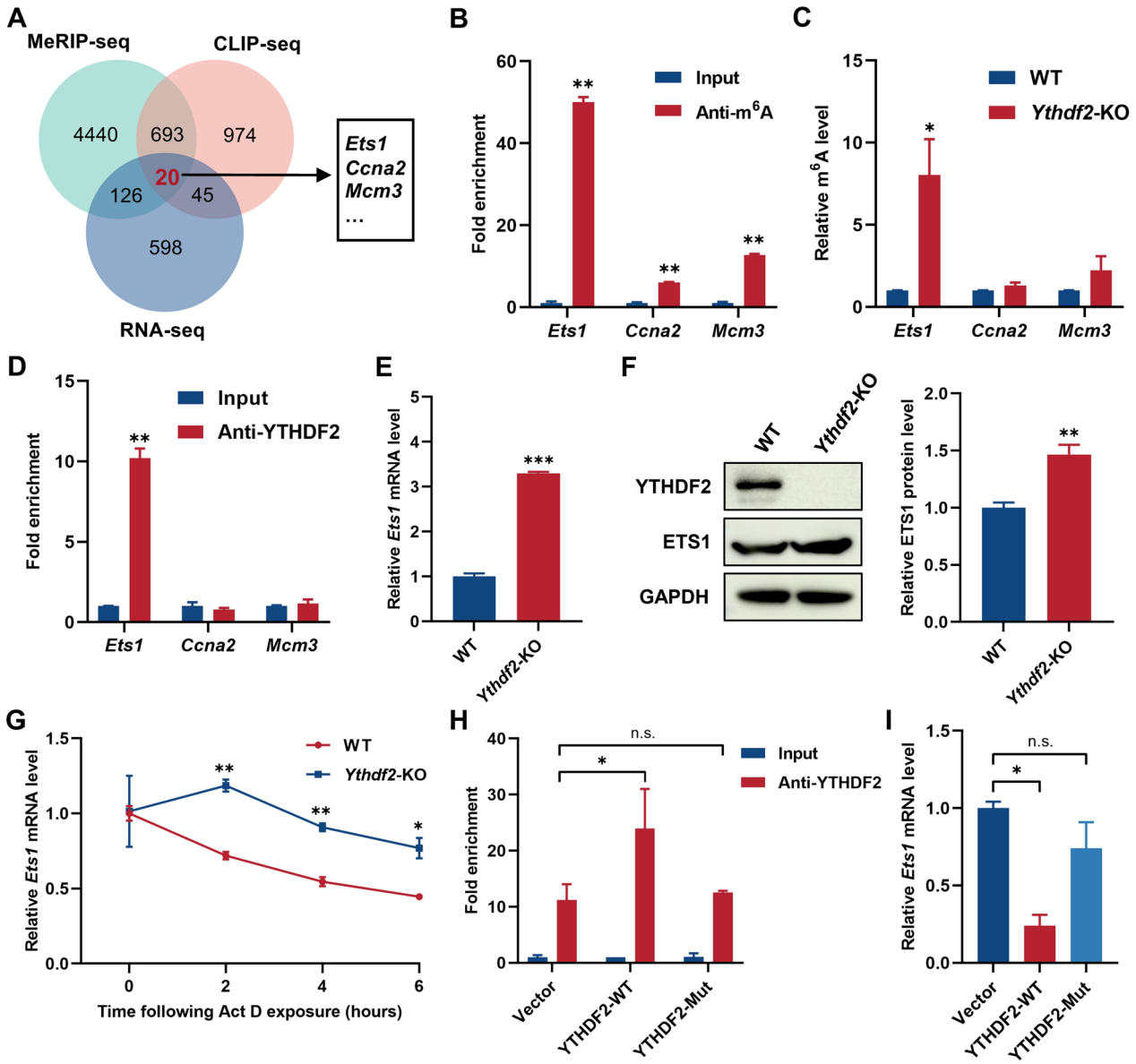

Fig. 3 YTHDF2 destabilizes *Ets1* mRNA in an m^{6}A-dependent manner. **a** Venn diagram showing the number of shared genes between MeRIP-seq, RNA-seq, and published YTHDF2 CLIP-seq data (GSE188846). **b** MeRIP-qPCR analysis of m^{6}A levels of *Ets1*, *Ccna2,* and *Mcm3* in WT cells. **c** MeRIP-qPCR analysis of m^{6}A levels of *Ets1*, *Ccna2,* and *Mcm3* in WT and *Ythdf2*-KO cells. **d** RIP-qPCR analysis of *Ets1*, *Ccna2,* and *Mcm3* in WT cells. **e** RT-qPCR analysis of *Ets1* mRNA in WT and *Ythdf2*-KO cells. **f** Western blotting analysis of ETS1 expression in WT and *Ythdf2*-KO cells. **g** RNA stability analysis of *Ets1* in WT and *Ythdf2*-KO cells. **h** RIP-qPCR analysis of YTHDF2-WT or YTHDF2-Mut binding on the *Ets1* mRNA. **i** RT-qPCR analysis of *Ets1* mRNA after expressing empty vector control (Vector), YTHDF2-WT, or YTHDF2-Mut in FGSCs. *$p < 0.05$, **$p < 0.01$, ***$p < 0.001$, n.s. $p > = 0.05$. Data are shown as mean ± SD

H3K18la promotes *Ythdf2* transcription in FGSCs

We then aimed to elucidate the potential mechanisms regulating YTHDF2 expression in FGSCs. Previous studies have demonstrated that stem cells predominantly rely on glycolysis for their energy supply [29–31]. Undifferentiated spermatogonia also exhibits a high glycolytic activity [32]. This metabolic process often results in substantial lactate production, which acts as substrates for histone lactylation. To ascertain the global/pan-lysine lactylation (pan-Kla) level in FGSCs, western blotting was performed in FGSCs and ovarian tissue. Compared with ovarian tissue, significantly higher pan-Kla levels were observed in FGSCs (Fig. 6a). Considering the recognized involvement of H3K18la in

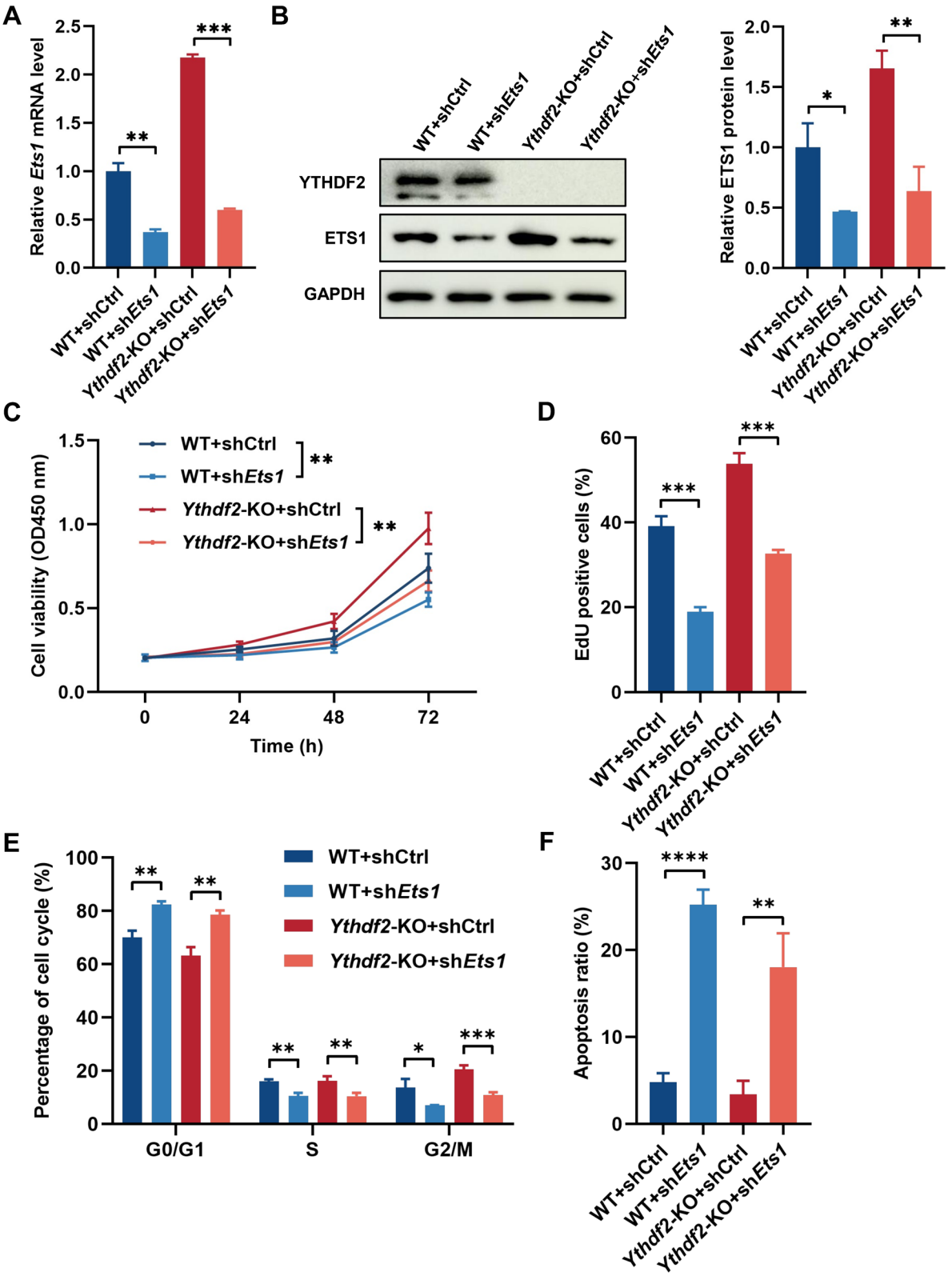

Fig. 4 ETS1 serves as a key downstream effector of YTHDF2 in regulating FGSC proliferation. **a** Knockdown efficiency of *Ets1* was detected by RT-qPCR. **b** Knockdown efficiency of *Ets1* was detected by western blotting. **c** Cell viability of ETS1 KD and negative control cells was detected using CCK-8 assay. **d** EdU staining of ETS1 KD and negative control cells. **e** Cell cycle analysis of ETS1 KD and negative control cells using flow cytometry. **f** TUNEL staining of ETS1 KD and negative control cells. *$p < 0.05$, **$p < 0.01$, ***$p < 0.001$, **** $p < 0.0001$. Data are shown as mean ± SD

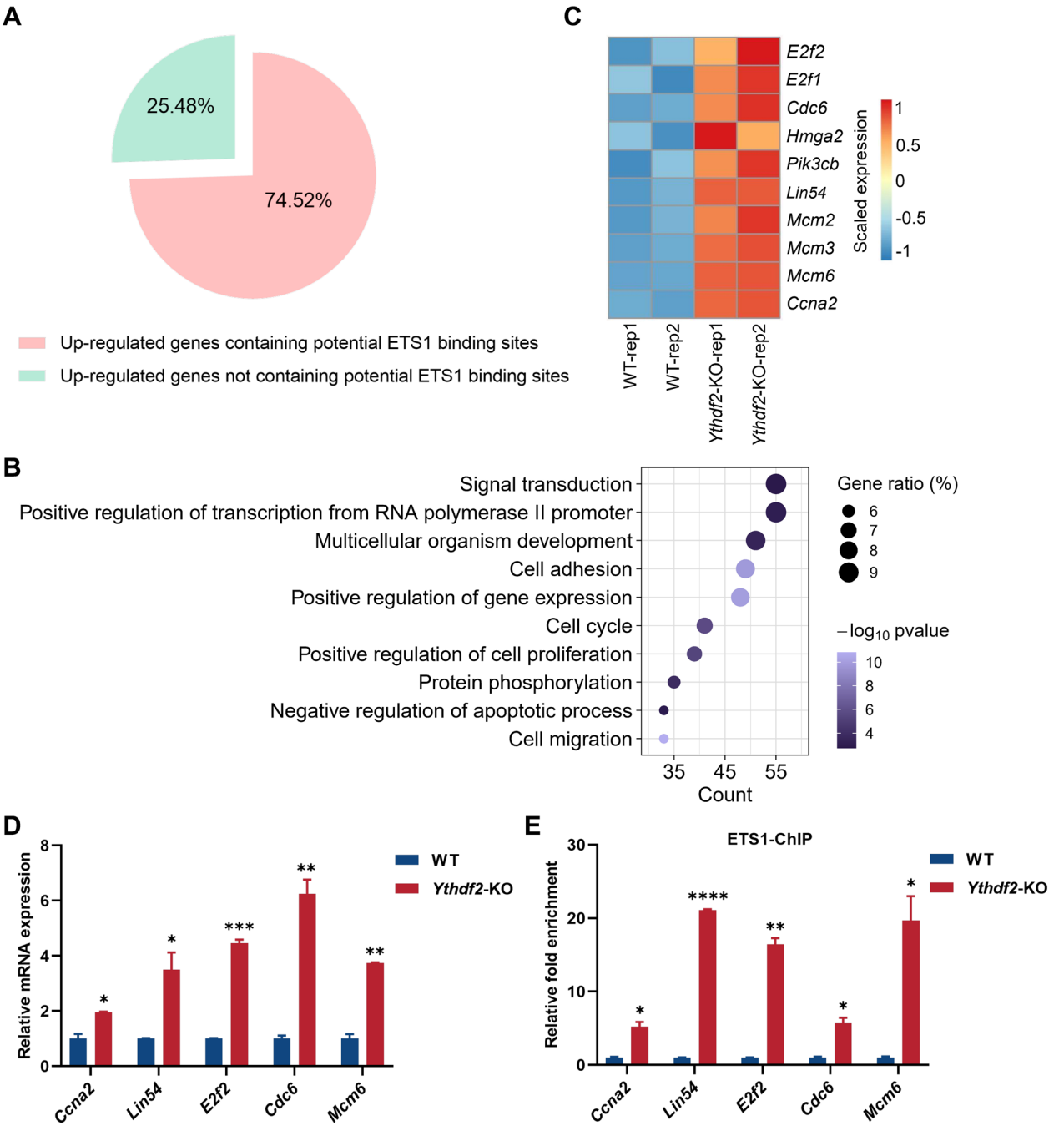

Fig. 5 YTHDF2/ETS1 axis participates in the regulation of FGSC proliferation. **a** Proportion of up-regulated genes containing potential ETS1-binding sites. **b** GO enrichment analysis of ETS1 potential target genes. **c** Heatmap of the scaled FPKM values of genes targeted by ETS1 in WT and *Ythdf2*-KO cells. **d** RT-qPCR detection of cell proliferation-related genes in WT and *Ythdf2*-KO cells. **e** ChIP-qPCR analysis of cell proliferation-related genes. * $p < 0.05$, ** $p < 0.01$, *** $p < 0.001$, **** $p < 0.0001$. Data are shown as mean ± SD

gene expression activation [33], we then examined the level of H3K18la in FGSCs. Consistently, FGSCs exhibit higher levels of H3K18la compared to ovarian tissue (Fig. 6b). Additionally, we observed the H3K18la modification at the promoter region of *Ythdf2*, suggesting a regulatory effect of histone lactylation on YTHDF2 expression (Fig. 6c).

To further validate the potential role of histone lactylation in facilitating YTHDF2 expression, we treated

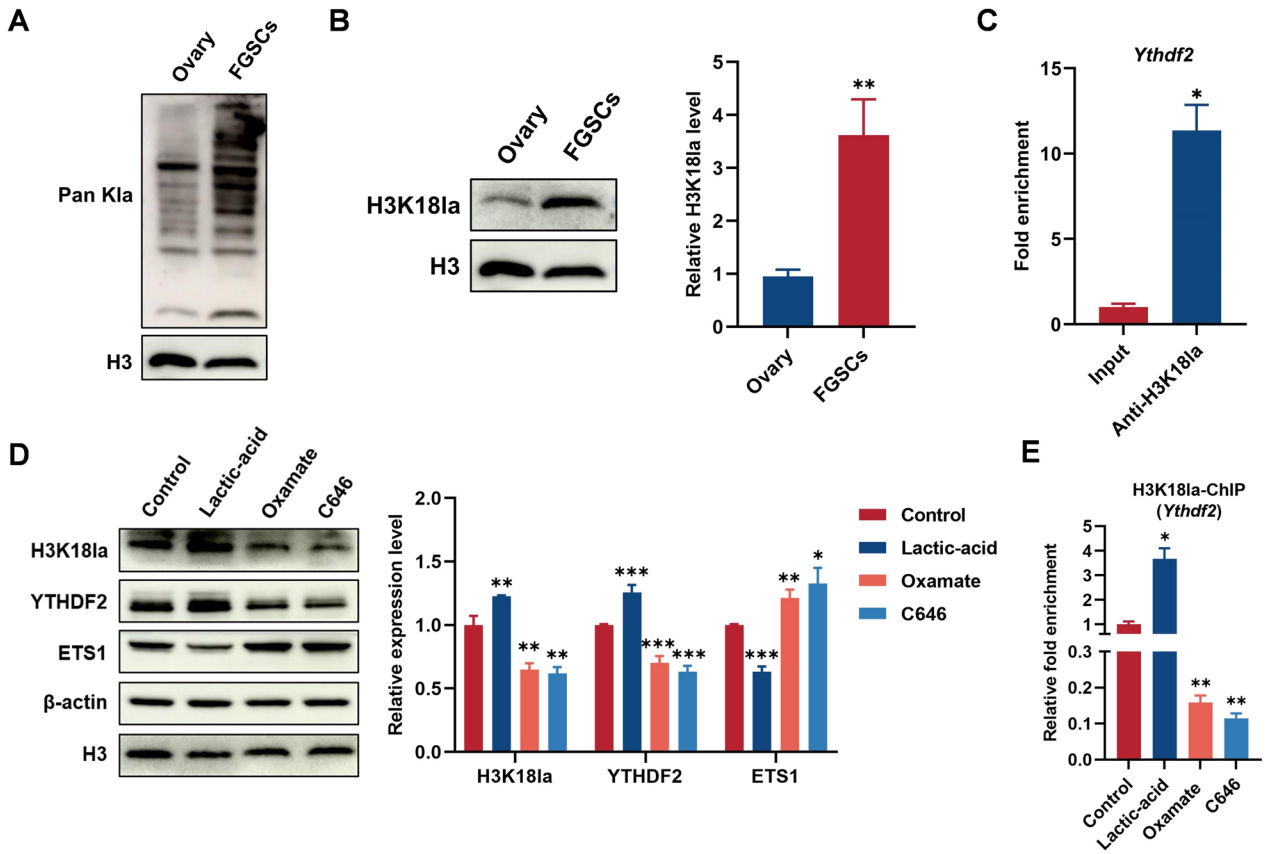

Fig. 6 H3K18la promotes *Ythdf2* transcription in FGSCs. **a** Pan Kla level was detected in ovary and FGSCs by western blotting. **b** H3K18la level was detected in ovary and FGSCs by western blotting. **c** ChIP-qPCR was used to determine enrichment of H3K18la at the promoter region of *Ythdf2* in FGSCs. **d** Western blotting analysis of H3K18la, YTHDF2, and ETS1 levels after treatment with lactic acid (25 mM), oxamate (20 mM), and C646 (10 μM) for 24 h in FGSCs. **e** ChIP-qPCR was used to determine the enrichment of H3K18la at the promoter region of *Ythdf2* after treatment with lactic acid (25 mM), oxamate (20 mM), and C646 (10 μM) for 24 h in FGSCs. *$p < 0.05$, **$p < 0.01$, ***$p < 0.001$, **** $p < 0.0001$. Data are shown as mean ± SD

FGSCs with lactic acid, oxamate (the inhibitor of LDHA), and C646 (the inhibitor of histone Kla 'writer' p300), respectively. After 24 h of treatment, lactic acid supplementation significantly increases the level of H3K18la in FGSCs, accompanied by an up-regulation of YTHDF2 expression and down-regulation of ETS1 expression (Fig. 6d). In contrast, both oxamate and C646 treatments lead to a decrease in the level of H3K18la, along with a reduction in YTHDF2 expression and an increase in ETS1 expression (Fig. 6d). Additionally, we found a significant increase of H3K18la modification level at the promoter region of *Ythdf2* following treatment with lactic acid, while that was notably decreased following treatment with both oxamate and C646 (Fig. 6e). Taken together, these observations indicate that H3K18la modification at the *Ythdf2* locus promotes its expression in FGSCs.

Discussion

Infertility affects a considerable number of couples worldwide [1]. Deficiency of functional oocytes accounts for the major factors of female infertility and even blocks the chance of in vitro fertilization. Germline stem cells offer a promising avenue for infertility treatment [34, 35]. FGSCs have been isolated from various species by our research group and other groups [34, 36]. However, the rare number of FGSCs in the mammalian ovary hinders their research and application. Understanding both extrinsic and intrinsic mechanisms that affecting FGSC expansion is critical for its potential clinical application. Additionally, we observed a significant increase of H3K18la modification at the promoter region of *Ythdf2* following treatment with lactic acid, while that was notably decreased following treatment with both oxamate and C646. In our previous studies, we found that GDNF activates FGSC self-renewal via the PI3K-AKT pathway through its receptor GFRA1 on the surface of

FGSCs [37], and CDH22 can similarly activate FGSC self-renewal through the PI3K-AKT pathway and β-catenin independently [37, 38]. Moreover, we also found that metformin and natural phytoestrogen isoflavone daidzein promote FGSC proliferation [39, 40]. However, the mechanisms inhibiting FGSC proliferation remain unclear. In this study, we reported the epigenetic factor YTHDF2 as an intrinsic regulator that restrains FGSC proliferation.

m^{6}A RNA epigenetic modification plays an important role in the development of germ cells. Germ cell-specific knockout of m^{6}A writers *Mettl3* or *Mettl14* leads to mRNA translation dysregulation, thus affecting spermatogonial stem cell proliferation [41]. Our recent studies also observed that m^{6}A regulators YTHDF1 and METTL14 promote FGSC self-renewal [16, 42]. Our current study found that YTHDF2 acts as a negative regulator of ETS1, and demonstrated that YTHDF2/ETS1 axis restrains FGSC proliferation. Considering diminished ovarian reserve and dysfunctional oogenesis are major causes of infertility, our study provides a significant promise for clinical applications in treating female infertility.

Transcription factor ETS1 has been reported to be involved in regulating stem cell proliferation. In human limbal epithelial stem cells (LESCs), ETS1 promotes LESC proliferation by activating chromatin regulator HMGA2 [25]. In this study, we found that ETS1 exerts a similar effect on mouse FGSCs. Rather than activating chromatin regulator, we observed that ETS1 promotes FGSC proliferation by up-regulating the expression of proliferation-related genes. Moreover, this study demonstrated that YTHDF2 negatively regulates m^{6}A-modified *Ets1* mRNA to hold its expression at a moderate level, thus restraining FGSC proliferation. Our findings offer a new perspective regarding the mechanism of ETS1-mediated regulation of stem cell proliferation.

Both ESCs and adult stem cells maintain a high level of glycolysis to support the production of essential building blocks such as nucleotides, phospholipids, and amino acids, as well as to meet their energy demands [29–31]. Glycolysis is critical for the maintenance of self-renewal in stem cells [43–48]. Furthermore, undifferentiated

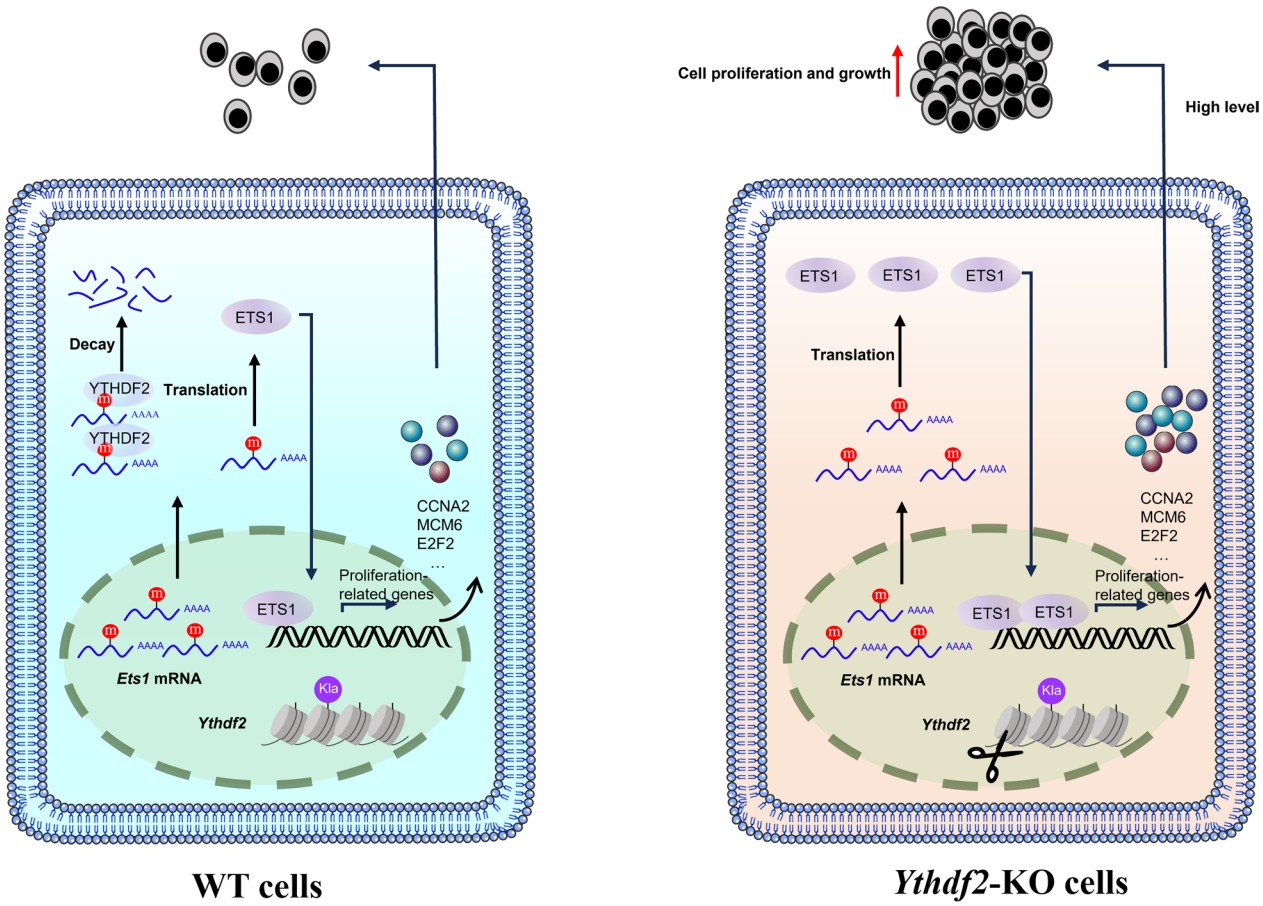

Fig. 7 Working model showing YTHDF2 restrains FGSC proliferation by destabilizing m^{6}A-modified *Ets1* mRNA

spermatogonia exhibit a higher glycolytic capacity, while inhibition of glycolysis suppressed long-term SSC growth and maintenance [32]. Lactate, which is produced during glycolysis, serves as a substrate for histone modification [33]. In this study, we demonstrated that FGSCs show a high level of pan-Kla and H3K18la. Moreover, lactate-mediated histone modification enhances YTHDF2 expression and subsequently restrains cell proliferation in FGSCs (Fig. 7). These findings indicate a link between histone lactylation and cellular proliferation of FGSCs.

Conclusion

In summary, this study reveals an intrinsic mechanism by which YTHDF2 destabilizes m^{6}A-modified *Ets1* mRNA and thus restrains FGSC proliferation. Moreover, histone lactylation promotes the expression of YTHDF2 in FGSCs. These findings provide evidence to further the understanding of the regulatory mechanisms governing FGSC proliferation and pave the way for the development of therapeutic strategies that improve fertility.

Abbreviations

m^{6}A	N^6-Methyladenosine
FGSC	Female germline stem cell
RNA-seq	RNA sequencing
GO	Gene ontology
GSEA	Gene set enrichment analysis
MeRIP-seq	Methylated RNA immunoprecipitation sequencing
CLIP-seq	Cross-linking immunoprecipitation and high-throughput sequencing
RT-PCR	Reverse transcription polymerase chain reaction
RT-qPCR	Real-time quantitative polymerase chain reaction
ChIP-qPCR	Chromatin immunoprecipitation coupled with qPCR
MEM-α	Minimum essential medium-α
FBS	Fetal bovine serum
NEAA	Nonessential amino acid
EGF	Epidermal growth factor
LIF	Leukemia inhibitory factor
GDNF	Glial cell line-derived neurotrophic factor
bFGF	Basic fibroblast growth factor
DMEM	Dulbecco's modified Eagle's medium
FPKM	Fragments per kilobase of exon per million fragments mapped
RIP-qPCR	RNA immunoprecipitation-qPCR

Supplementary Information

The online version contains supplementary material available at https://doi.org/10.1186/s13148-025-01890-4.

Additional file1 (DOCX 3732 kb)

Acknowledgements

We thank Genefund Biotech (Shanghai, China) for the assistance in deep-sequencing data analysis. We thank Sheng Tan and Simin Luo for sharing plasmid used in this study.

Author contributions

YQW performed the major experiments and data analyses and wrote the manuscript. BX, YLP, and JW analyzed data. SL, WFD, RQL, and SZ assisted in the experiment. XDZ initiated and supervised the project. KZ and XDZ revised the manuscript. All authors read and approved the final manuscript.

Funding

This work was supported by the National Key Research and Development Program of China (2024YFA1108100).

Availability of data and material

All sequencing data generated for this study have been deposited in the ArrayExpress Database, and could be accessed with the links https://www.ebi.ac.uk/biostudies/arrayexpress/studies/E-MTAB-14257?key=841381b8-b021-4633-b49e-3ded13d4e617 for RNA-seq data and https://www.ebi.ac.uk/biostudies/arrayexpress/studies/E-MTAB-14256?key=35c23a1e-b530-476f-b245-e04fb763c5d4 for MeRIP-seq data. The published data (GSE188846) used in this paper are available in Gene Expression Omnibus (GEO) database [23].

Declarations

Ethics approval

This entire study was approved by the Institutional Animal Care and Use Committee (IACUC) of Shanghai Jiao Tong University.

Consent for publication

Not applicable.

Competing interests

The authors declare no competing interests.

Received: 20 March 2025 Accepted: 30 April 2025
Published online: 27 May 2025

References

1. Inhorn MC, Patrizio P. Infertility around the globe: new thinking on gender, reproductive technologies and global movements in the 21st century. Hum Reprod Update. 2015;21(4):411–26.
2. Eisenberg ML, Esteves SC, Lamb DJ, Hotaling JM, Giwercman A, Hwang K, Cheng Y-S. Male infertility. Nat Rev Dis Primers. 2023;9(1):49.
3. Zou K, Yuan Z, Yang Z, Luo H, Sun K, Zhou L, Xiang J, Shi L, Yu Q, Zhang Y, et al. Production of offspring from a germline stem cell line derived from neonatal ovaries. Nat Cell Biol. 2009;11(5):631–6.
4. Zhou L, Wang L, Kang JX, Xie W, Li X, Wu C, Xu B, Wu J. Production of fat-1 transgenic rats using a post-natal female germline stem cell line. Mol Hum Reprod. 2014;20(3):271–81.
5. Zou K, Hou L, Sun K, Xie W, Wu J. Improved efficiency of female germline stem cell purification using fragilis-based magnetic bead sorting. Stem Cells Dev. 2011;20(12):2197–204.
6. Dominissini D, Moshitch-Moshkovitz S, Schwartz S, Salmon-Divon M, Ungar L, Osenberg S, Cesarkas K, Jacob-Hirsch J, Amariglio N, Kupiec M, et al. Topology of the human and mouse m6A RNA methylomes revealed by m6A-seq. Nature. 2012;485(7397):201–6.
7. Wang X, Lu Z, Gomez A, Hon GC, Yue Y, Han D, Fu Y, Parisien M, Dai Q, Jia G, et al. N^6-methyladenosine-dependent regulation of messenger RNA stability. Nature. 2014;505(7481):117–20.
8. Wang X, Zhao BS, Roundtree IA, Lu Z, Han D, Ma H, Weng X, Chen K, Shi H, He C. N(6)-methyladenosine modulates messenger RNA translation efficiency. Cell. 2015;161(6):1388–99.
9. Zheng G, Dahl JA, Niu Y, Fedorcsak P, Huang C-M, Li CJ, Vågbø CB, Shi Y, Wang W-L, Song S-H, et al. ALKBH5 is a mammalian RNA demethylase that impacts RNA metabolism and mouse fertility. Mol Cell. 2013;49(1):18–29.
10. Zaccara S, Ries RJ, Jaffrey SR. Reading, writing and erasing mRNA methylation. Nat Rev Mol Cell Biol. 2019;20(10):608–24.
11. Yang Y, Hsu PJ, Chen Y-S, Yang Y-G. Dynamic transcriptomic m6A decoration: writers, erasers, readers and functions in RNA metabolism. Cell Res. 2018;28(6):616–24.
12. Shi H, Wei J, He C. Where, when, and how: context-dependent functions of RNA methylation writers, readers, and erasers. Mol Cell. 2019;74(4):640–50.

13. Mu H, Zhang T, Yang Y, Zhang D, Gao J, Li J, Yue L, Gao D, Shi B, Han Y, et al. METTL3-mediated mRNA N^6-methyladenosine is required for oocyte and follicle development in mice. Cell Death Dis. 2021;12(11):989.
14. Hu Y, Ouyang Z, Sui X, Qi M, Li M, He Y, Cao Y, Cao Q, Lu Q, Zhou S, et al. Oocyte competence is maintained by m6A methyltransferase KIAA1429-mediated RNA metabolism during mouse follicular development. Cell Death Differ. 2020;27(8):2468–83.
15. Kasowitz SD, Ma J, Anderson SJ, Leu NA, Xu Y, Gregory BD, Schultz RM, Wang PJ. Nuclear m6A reader YTHDC1 regulates alternative polyadenylation and splicing during mouse oocyte development. PLoS Genet. 2018;14(5): e1007412.
16. Zhao X, Tian GG, Fang Q, Pei X, Wang Z, Wu J. Comparison of RNA m6A and DNA methylation profiles between mouse female germline stem cells and STO cells. Mol Ther Nucl Acids. 2021;23:431–9.
17. Ivanova I, Much C, Di Giacomo M, Azzi C, Morgan M, Moreira PN, Monahan J, Carrieri C, Enright AJ, O'Carroll D. The RNA mA reader YTHDF2 is essential for the post-transcriptional regulation of the maternal transcriptome and oocyte competence. Molecular cell. 2017;67(6):
18. Zhang X-L, Wu J, Wang J, Shen T, Li H, Lu J, Gu Y, Kang Y, Wong C-H, Ngan CY, et al. Integrative epigenomic analysis reveals unique epigenetic signatures involved in unipotency of mouse female germline stem cells. Genome Biol. 2016;17(1):162.
19. Liu T, Wei Q, Jin J, Luo Q, Liu Y, Yang Y, Cheng C, Li L, Pi J, Si Y, et al. The m6A reader YTHDF1 promotes ovarian cancer progression via augmenting EIF3C translation. Nucl Acids Res. 2020;48(7):3816–31.
20. Liu R, Peng Y, Du W, Wu Y, Zhang W, Hu C, Liu M, Liu X, Wu J, Sun J, et al. BMI1 fine-tunes gene repression and activation to safeguard undifferentiated spermatogonia fate. Front Cell Dev Biol. 2023;11:1146849.
21. Wang L, Dou X, Chen S, Yu X, Huang X, Zhang L, Chen Y, Wang J, Yang K, Bugno J *et al*. YTHDF2 inhibition potentiates radiotherapy antitumor efficacy. Cancer Cell. 2023;41(7):
22. Du H, Zhao Y, He J, Zhang Y, Xi H, Liu M, Ma J, Wu L. YTHDF2 destabilizes m(6)A-containing RNA through direct recruitment of the CCR4-NOT deadenylase complex. Nat Commun. 2016;7:12626.
23. Ito-Kureha T, Leoni C, Borland K, Cantini G, Bataclan M, Metzger RN, Ammann G, Krug AB, Marsico A, Kaiser S, et al. The function of Wtap in N6-adenosine methylation of mRNAs controls T cell receptor signaling and survival of T cells. Nat Immunol. 2022;23(8):1208–21.
24. Feng Y-R, Raza SHA, Liang C-C, Wang X-Y, Wang J-F, Zhang W-Z, Zan L. CREB1 promotes proliferation and differentiation by mediating the transcription of CCNA2 and MYOG in bovine myoblasts. Int J Biol Macromol. 2022;216:32–41.
25. Wang B, Guo H, Liu D, Wu S, Liu J, Lan X, Huang H, An F, Zhu J, Ji J, et al. ETS1-HMGA2 Axis Promotes Human Limbal Epithelial Stem Cell Proliferation. Invest Ophthalmol Vis Sci. 2023;64(1):12.
26. Zhou H, Xiong Y, Zhang G, Liu Z, Li L, Hou S, Zhou T. Elevated expression of minichromosome maintenance 3 indicates poor outcomes and promotes G1/S cell cycle progression, proliferation, migration and invasion in colorectal cancer. Biosci Rep. 2020;40(7).
27. Zhu T, Roundtree IA, Wang P, Wang X, Wang L, Sun C, Tian Y, Li J, He C, Xu Y. Crystal structure of the YTH domain of YTHDF2 reveals mechanism for recognition of N^6-methyladenosine. Cell Res. 2014;24(12):1493–6.
28. Grant CE, Bailey TL, Noble WS. FIMO: scanning for occurrences of a given motif. Bioinformatics. 2011;27(7):1017–8.
29. Chen C-T, Shih Y-RV, Kuo TK, Lee OK, Wei Y-H. Coordinated changes of mitochondrial biogenesis and antioxidant enzymes during osteogenic differentiation of human mesenchymal stem cells. Stem Cells. 2008;26(4):960–8.
30. Mathieu J, Ruohola-Baker H. Metabolic remodeling during the loss and acquisition of pluripotency. Development. 2017;144(4):541–51.
31. Zhang J, Khvorostov I, Hong JS, Oktay Y, Vergnes L, Nuebel E, Wahjudi PN, Setoguchi K, Wang G, Do A, et al. UCP2 regulates energy metabolism and differentiation potential of human pluripotent stem cells. EMBO J. 2011;30(24):4860–73.
32. Chen W, Zhang Z, Chang C, Yang Z, Wang P, Fu H, Wei X, Chen E, Tan S, Huang W, et al. A bioenergetic shift is required for spermatogonial differentiation. Cell Discov. 2020;6:56.
33. Zhang D, Tang Z, Huang H, Zhou G, Cui C, Weng Y, Liu W, Kim S, Lee S, Perez-Neut M, et al. Metabolic regulation of gene expression by histone lactylation. Nature. 2019;574(7779):575–80.
34. Cheng H, Shang D, Zhou R. Germline stem cells in human. Signal Transduct Target Ther. 2022;7(1):345.
35. Wu J-X, Xia T, She L-P, Lin S, Luo X-M. Stem cell therapies for human infertility: advantages and challenges. Cell Transplant. 2022;31:9636897221083252.
36. Hong W, Wang B, Zhu Y, Je Wu, Qiu L, Ling S, Zhou Z, Dai Y, Zhong Z, Zheng Y. Female germline stem cells: aging and anti-aging. J Ovarian Res. 2022;15(1):79.
37. Zhang X, Wei R, Sun Y, Xia Q, Xie W, Song H, Wang W, Zou K. AKT3 is a pivotal molecule of cadherin-22 and GDNF family receptor-α1 signal pathways regulating self-renewal in female germline stem cells. Stem Cells. 2019;37(8):1095–107.
38. Zhang X, Yang Y, Xia Q, Song H, Wei R, Wang J, Zou K. Cadherin 22 participates in the self-renewal of mouse female germ line stem cells via interaction with JAK2 and β-catenin. Cell Mol Life Sci. 2018;75(7):1241–53.
39. Wang X, Tian GG, Cheng W, Yu X, Li X, Wu J. Metformin promotes female germline stem cell proliferation by upregulating Gata-binding protein 2 with histone β-hydroxybutyrylation. Stem Cell Res Ther. 2023;14(1):144.
40. Li F, Hu X, Wu J. Daidzein activates akt pathway to promote the proliferation of female germline stem cells through upregulating Clec11a. Stem Cell Rev Rep. 2022;18(8):3021–32.
41. Lin Z, Hsu PJ, Xing X, Fang J, Lu Z, Zou Q, Zhang K-J, Zhang X, Zhou Y, Zhang T, et al. Mettl3-/Mettl14-mediated mRNA N^6-methyladenosine modulates murine spermatogenesis. Cell Res. 2017;27(10):1216–30.
42. Li X, Tian G, Wu J. Novel circGFRα1 promotes self-renewal of female germline stem cells mediated by m6A writer METTL14. Front Cell Dev Biol. 2021;9:640402.
43. Cliff TS, Dalton S. Metabolic switching and cell fate decisions: implications for pluripotency, reprogramming and development. Curr Opin Genet Dev. 2017;46:44–9.
44. Dong Q, Zhang Q, Yang X, Nai S, Du X, Chen L. Glycolysis-stimulated esrrb lactylation promotes the self-renewal and extraembryonic endoderm stem cell differentiation of embryonic stem cells. Int J Mol Sci. 2024;25(5).
45. Kondoh H, Lleonart ME, Nakashima Y, Yokode M, Tanaka M, Bernard D, Gil J, Beach D. A high glycolytic flux supports the proliferative potential of murine embryonic stem cells. Antioxid Redox Signal. 2007;9(3):293–9.
46. Li C, Zhou Y, Wei R, Napier DL, Sengoku T, Alstott MC, Liu J, Wang C, Zaytseva YY, Weiss HL, et al. Glycolytic regulation of intestinal stem cell self-renewal and differentiation. Cell Mol Gastroenterol Hepatol. 2023;15(4):931–47.
47. Theret M, Gsaier L, Schaffer B, Juban G, Ben Larbi S, Weiss-Gayet M, Bultot L, Collodet C, Foretz M, Desplanches D, et al. AMPKα1-LDH pathway regulates muscle stem cell self-renewal by controlling metabolic homeostasis. EMBO J. 2017;36(13):1946–62.
48. Zhang J, Nuebel E, Daley GQ, Koehler CM, Teitell MA. Metabolic regulation in pluripotent stem cells during reprogramming and self-renewal. Cell Stem Cell. 2012;11(5):589–95.

Publisher's Note